ELSEVIER

Contents lists available at ScienceDirect

Chemical Engineering Journal

journal homepage: www.elsevier.com/locate/cej





Rapid carbon-free iron ore reduction using an atmospheric pressure hydrogen microwave plasma

Sachin Kumar¹, Zichang Xiong¹, Julian Held, Peter Bruggeman, Uwe R. Kortshagen *

Department of Mechanical Engineering, University of Minnesota, USA

ARTICLE INFO

Keywords: Iron ore reduction Green steelmaking Hydrogen plasma Atmospheric pressure plasma Microwave

ABSTRACT

 CO_2 emissions from steel production account for about 8% of the global anthropogenic CO_2 emissions and the majority (over 70%) of these emissions occur during the reduction of iron ore to iron. Hence, the steel industry is striving to reduce its dependence on carbon-based energy sources and reducing agents, like the coke used in a traditional blast furnace. Approaches such as hydrogen-based direct reduction are being considered since they can drastically reduce the overall CO_2 emissions of the steel-making process. Here, we report an electrified process for reducing iron ore particles using atmospheric pressure hydrogen plasma powered by microwave energy. The process has the potential to be entirely carbon-free and overcome common challenges of other hydrogen reduction approaches, including other plasma-based approaches. Relative reduction rates achieved are as high as 15.5 %/s, on par or faster than the highest rates reported in the literature operating at lower temperatures and hydrogen concentrations. When compared to thermal reduction under otherwise close to identical conditions, the microwave plasma reduction is three to four times faster, suggesting the importance of plasma generated reactive species like atomic hydrogen. A promising mass scaling is observed, with increasing the mass load 50 times requiring only 7 times longer reaction, which points to a good potential for further scale-up of the technology.

1. Introduction

Steel is currently produced worldwide at a rate of 2 billion tons per year. For every ton of steel produced, the steel industry emits 1.9 tons of CO_2 , contributing roughly 8% of the global anthropogenic CO_2 emissions [1]. A large part of these CO_2 emissions (over 70%) occurs during the reduction of iron ore to pure iron or pig iron, which is the feedstock for steelmaking [2]. Currently, iron ore reduction is mostly performed in blast furnaces, using a carbon based reduction agent, like carbon monoxide (CO) released from coke. This reduction agent reacts with the iron ore, forming CO_2 as the by-product:

$$Fe_2O_3 + 3CO \rightarrow 2Fe + 3CO_2 \tag{1}$$

The International Energy Agency estimates that the steel industry must reduce their carbon emissions by 93% by 2050, relative to 2020, in order to achieve the aim of the Paris Agreement, i.e. limit the rise in global temperature to $1.5\,^{\circ}\text{C}$ above the pre-industrial levels [3]. Emerging technologies like carbon capture and utilization (CCU) [4,5], hydrogen-based reduction [6–8], and molten oxide electrolysis [9] are anticipated to play a key role in decarbonizing the steel industry.

The electrochemical reduction of iron ore to iron in alkaline media is another emerging technology for green steel production offering the advantages of low-temperature operation (373 K) and lower energy consumption (13 GJ t $^{-1}$ of Fe) [10,11]. The technology is estimated to potentially reduce CO $_2$ emissions by 87% and energy consumption by 31% when compared to traditional steelmaking. However, the technology faces some experimental challenges like a decrease in the system efficiency due to hydrogen evolution at the cathode and impurities in the ore hampering the electrochemical reduction [10].

Among the various technologies, the hydrogen-based reduction has become an attractive alternative because it emits water vapor instead of CO₂:

$$Fe_2O_3 + 3H_2 \rightarrow 2Fe + 3H_2O$$
 (2)

Hydrogen-based reduction of iron ore is a temperature-dependent multi-step process. At temperatures below 840 K, hematite (Fe_2O_3) is converted to magnetite (Fe_3O_4) and then to iron in the presence of hydrogen. However, at temperatures above 840 K, an intermediate

E-mail addresses: kumar749@umn.edu (S. Kumar), xion1832@umn.edu (Z. Xiong), jheld@umn.edu (J. Held), pbruggem@umn.edu (P. Bruggeman), korts001@umn.edu (U.R. Kortshagen).

^{*} Corresponding author.

¹ These authors contributed equally to this work and are listed in alphabetical order.

oxide wüstite (FeO) is formed as the reduction proceeds as [12]:

$$Fe_2O_3 \rightarrow Fe_3O_4 \rightarrow FeO \rightarrow Fe$$
 (3)

An attractive option for the steel industry is to include hydrogen as an auxiliary reducing agent in the carbon-based blast furnace reduction. Park et al. [13] showed that adding hydrogen in the blast furnace operation improves the gas utilization and coke gasification when compared to the conventional route of using CO as the sole reducing gas. In another study [14], simulation of a blast furnace predicted that the $\rm CO_2$ emissions can be reduced up to 21.4% by hydrogen injection when compared to the typical operation with pulverized coal as the sole reducing agent. However, adding hydrogen to the blast furnace increases the energy demand [15] and does not sufficiently reduce the emissions.

Alternatively, hot hydrogen can be used as the sole reduction agent, for example in shaft furnaces (Midrex, Energiron HYL [16,17]) or fluidized bed reactors (CIRCORED [18]). However, shaft furnace processes require iron ore pellets which are $10\,\mathrm{mm}$ to $12\,\mathrm{mm}$ in size. Pelletization adds to the energy demand (186–662 MJ/t pellet) and CO₂ emissions (17–193 kg CO₂/t pellet) of the process [19]. In contrast, fluidized bed reactors use iron ore fines, micrometer-sized particles of ground iron ore, avoiding the pelletization step, however, they suffer from particle sticking leading to defluidization and frequent breakdowns [20].

A promising approach might be the rapid in-flight reduction developed at the University of Utah. Here, small iron ore particles ($<100\,\mu m$) are heated to high temperatures of $1200\,^{\circ}\mathrm{C}$ to $1600\,^{\circ}\mathrm{C}$, enabling reduction within a few seconds, which makes the in-flight reduction possible [8]. Early lab-scale prototypes used an electric furnace to heat the particles [21]. However, the temperature that can be achieved with an electric furnace is limited and these systems often have a considerable thermal inertia, which is not a good match for intermittent sources of renewable electricity. Accordingly, a pilot reactor demonstrating the in-flight reduction at an iron ore feeding rate of 1–7 kg/h used combustion of natural gas or hydrogen as heat source [8,22].

Another method to heat the gas is using a solar-heated furnace. Li et al. [23] used solar-heated hydrogen gas to reduce hematite particles in a vibrating fluidized bed. High reduction (>90%) was achieved at temperatures as low as 770 K for particles with a mean size between $10\,\mu m$ to $15\,\mu m$ when the bed was vibrated at a frequency between $20\,Hz$ to $50\,Hz$. However, due to low operating temperatures, long reduction times of up to $50\,m$ in were needed for the reduction, and further investigations are needed to understand the industrial feasibility of the process.

Another alternative for volumetric gas heating is the use of an electrically-driven plasma. Here, the gas is directly heated by Joule heat rather by an external heating element, allowing to quickly start and stop the process and enabling temperatures on the order of 1000 K to 10 000 K without threatening the structural integrity of the reactor [24]. Moreover, plasmas also produce excited and reactive species, such as atomic hydrogen, ions, and vibrationally excited hydrogen molecules. These plasma-produced species were predicted to enable faster iron ore reduction at lower temperatures, when present at sufficient quantities. This is due to the lower Gibbs free energy change and activation energy of the reaction as compared to hot hydrogen gas [25]. In addition, atomic hydrogen and electron-ion recombination, and other exothermic reactions lead to surface heating [26,27] which can further improve the reduction rate of iron ore particles.

Ironmaking using thermal plasmas has already been demonstrated. In 1975, Bethlehem Steel Corporation developed a falling film reactor using a 1 MW direct current (DC) arc thermal plasma [25,28]. By using a 2:1 hydrogen–methane mixture, they claimed to produce iron from pulverized ore concentrates at an energy cost of $12\,\mathrm{GJ}\,t^{-1}\mathrm{Fe}$ [29], close to the theoretical minimum energy cost of producing pure iron with hydrogen of $6.5\,\mathrm{GJ}\,t^{-1}\,\mathrm{Fe}$ [25]. However, the technology was hampered by the short working lifetimes of the electrodes of the high-power plasma torch and challenges with further scale up [25].

Similarly, Plaul et al. used a thermal plasma arc to reduce iron ore fines, demonstrating a high degree of hydrogen utilization [30]. Currently, the SuSteel project explores the industrial application of this approach [31]. Further discussion on different plasma and non-plasma processes for hydrogen-based reduction of iron ore can be found in the review paper of Sabat and Murphy [25]. Also, a detailed comparison in the context of the typical reduction rates and operating parameters relevant to our work is reported in Section 3.5.

Generally, in thermal arc processes the hot plasma is in direct contact with an electrode. High heat fluxes limit the electrode lifetime, necessitating regular plasma source maintenance and potentially leading to contamination of the produced iron with evaporated electrode material [25]. In contrast, a microwave (MW) power source enables the electrode-less coupling of electrical power into the plasma, potentially extending plasma reactor lifetimes. Modern magnetrons can achieve an energy efficiency of 90% and can reach a power of 100 kW [32,33], allowing for further scale up. However, to our knowledge, the iron ore reduction using MW plasma has so far only been reported at sub-ambient pressure [34–36], which requires costly vacuum equipment and long process times associated with the pumping and venting between each reduction cycle. For a potential industrial application, operation at atmospheric pressure is needed.

Here, we report the reduction of iron ore fines using an atmospheric pressure MW plasma, overcoming many of the above inherent challenges, including the need for iron ore pellets, electrode erosion, and vacuum operation. Because of its small thermal inertia and volumetric gas heating provided by the plasma, the process is compatible with intermittent renewable energy sources such as wind and solar energy. By avoiding combustion as the heat source, the process does not produce ${\rm CO_2}$ and avoids additional ${\rm H_2O}$ production which shifts the equilibrium towards oxidation instead of reduction.

2. Methods

To asses the iron ore reduction using the microwave (MW) plasma, we compare two different methods: (i) an atmospheric pressure MW plasma and (ii) a thermal reduction process using the same argonhydrogen gas mixture, heated inside an electric furnace.

2.1. Microwave plasma reduction

Fig. 1 shows a detailed schematic of the reactor used for the MW plasma-based reduction along with a picture of the plasma column obtained at 45 slm and 1.7 kW. A magnetron was used to generate microwaves at 2.45 GHz, which were then directed through a circulator into a waveguide. The MW power was measured using a directional coupler and power meter (Anritsu ML2438a). The forward power was set to 1.8 kW, while the reflected power varied only slightly between 120 W and 160 W depending on the discharge conditions. Thus, the net discharge power was about 1.7 kW in all experiments reported in this work.

The plasma source used was a surfaguide with a tapered waveguide designed to intensify the electric field and enable an easier ignition at atmospheric pressure. A quartz tube with a 22 mm inner diameter crossed through a hole in the tapered waveguide and allowed the microwaves to interact with the gas flow. An argon-hydrogen gas mixture (90:10 volume %) entered the quartz tube from the top at flow rates between 20 slm and 45 slm (standard liter per minute). Argon is used to dilute the hydrogen concentration, ensuring safe operation for the prototype reactor reported in this work without affecting the reduction chemistry due to its inert behavior, unlike, for example, nitrogen which can be dissociated or ionized by the plasma and then react with the hydrogen. However, for an industrial application, the process would likely be operated in pure hydrogen. A small part of the total gas flow entered the quartz tube in the axial direction (5 slm) while the rest was injected tangentially through two side ports at the inlet

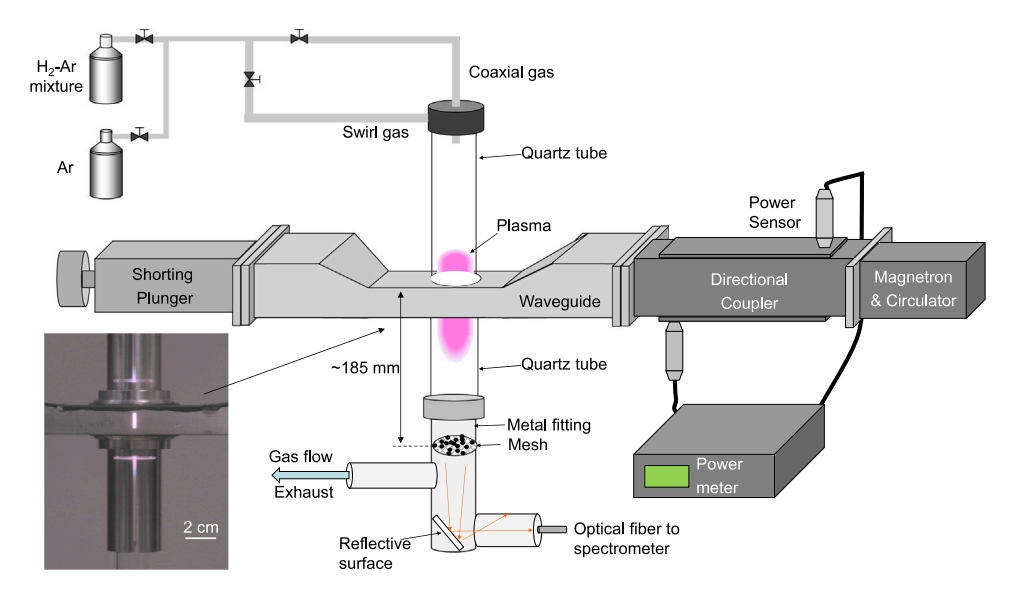


Fig. 1. Experimental setup for microwave plasma iron-ore reduction along with an insert of plasma emission at 45 slm.

to create a swirl flow that stabilized the plasma and reduced the heat flux to the walls [37]. The plasma was ignited using a sharp tungsten tip that was inserted into the reactor from the bottom and removed after ignition. The bright optical plasma emission, shown in Fig. 1, is confined to a narrow region in the center of the quartz tube with a length of around 60 mm. Flow rate variations from 30 slm to 45 slm caused a negligible change in the plasma emission, shown in figure S5 supplementary information.

The plasma heats the gas and plasma electrons create reactive hydrogen atoms, ions, and vibrationally excited molecules which are carried along the gas flow. This plasma effluent was then directed onto iron ore particles resting on a stainless steel mesh (400 mesh, hole size of 37 µm), placed below the plasma at a distance of 185 mm from the top of the waveguide. The mesh allowed the flow to pass through the iron ore powder, enabling efficient interaction between particles and gas. The distance between the visible plasma edge and the particles was estimated to be about 140 mm. This study mostly focuses on magnetite particles with an average size <5 µm, purchased from Millipore Sigma with product number: 310069. The BET surface area of the magnetite particles used in this study was measured to be $(4.34 \pm 0.03) \, \text{m}^2 \, \text{g}^{-1}$. The experimental details of the BET analysis can be found in [38]. For comparison, hematite particles (<5 µm, Millipore Sigma, product number: 310050) and natural iron ore particles (~30 µm, Alpha Chemicals) were also used. The natural iron ore was manually sieved to a size below

The sample treatment was performed by first igniting the plasma at 5 slm pure argon gas flow and 1.4 kW MW power. Low flow rates, low input MW power, and less efficient coupling of MW power to argon flow reduced early particle heating before the hydrogen plasma treatment starts. Consequently, the temperature during this first step was only about 440 K. Next, gas flow and MW power were increased to the desired values, while still flowing pure argon, increasing the temperature to about 600 K. The gas flow was then quickly switched to the argon-hydrogen mixture, starting the reduction process. After the desired treatment time, the gas flow was switched back to pure argon and the plasma terminated. A cooling argon gas flow was maintained for a while, to cool the particles below the temperature at which a possible re-oxidation might occur when exposed to air. Re-oxidation was tested by performing the treatment of a 10 mg sample for an excessive time of 30 s, thus ensuring ~100 % reduction. Since no traces of oxides were detected in the XRD measurements for the above sample on exposure to ambient, we conclude that re-oxidation of Fe is not essential, though we cannot exclude the presence of a thin, likely nanometer-scale, layer of an amorphous native oxide.

2.2. Thermal reduction

To facilitate a comparison between the MW plasma reduction and a purely thermal hydrogen reduction, the setup shown in Fig. 2 was used. It consisted of an electric furnace (Thermo Scientific Lindberg/Blue M STF55346C) with a steel tube of 35 mm inner diameter passing through the heating zone. The same argon–hydrogen (90:10 volume %) gas mixture was used as in the MW plasma reduction, flowing at a rate of 35 slm. Crumpled-up stainless steel mesh was placed in the path of the gas before it interacted with the iron ore particles to enhance the heat transfer. A mass of 10 mg of magnetite particles were placed inside a cup formed from the stainless steel mesh and attached to a push rod. The push rod allowed the introduction of particles into the furnace once the desired temperature was achieved.

To perform the reduction, initially, pure argon was flowed through the tube while introducing particles into the furnace. Once the particles reached the desired position in the middle of the furnace, the flow was switched to the argon–hydrogen mixture. After the desired treatment time was achieved, the flow was switched back to pure argon, thus terminating the reduction process. The particles were then pulled out of the furnace heating zone. The main flow was turned off and a cooling flow of pure argon, not passing the heating zone of the furnace, was used to lower the particle temperature to prevent a possible re-oxidation upon air exposure. No oxides were found when a fully reduced sample after 3 min treatment time at 1350 K was exposed to ambient, demonstrating that no re-oxidation of Fe occurred. Gas temperatures during the reduction process were varied between 1200 K and 1350 K to explore the temperature dependence of the reduction.

2.3. Temperature measurements

For the MW plasma reduction, the glow of particles and the mesh on which particles were resting was reflected on aluminum foil placed at the bottom of the reactor and then coupled into a spectrometer (Avaspec ULS4096CL-RS-EVO) using an optical fiber (Avantes FC-UVIR600-2), as shown in Fig. 1. Due to the multiple internal reflections of the radiation from the mesh/particles in the reactor tubes, the aluminum foil acted more as a diffuser than as a mirror. It was observed that only the mesh and the particles on the mesh emit light in the visible range during the experiment. Because of the good thermal contact, we assume the mesh and particle temperature to be equal. Since the total emissive power of a black body increases with temperature to the fourth power, it was assumed that the hottest spot of the mesh is being

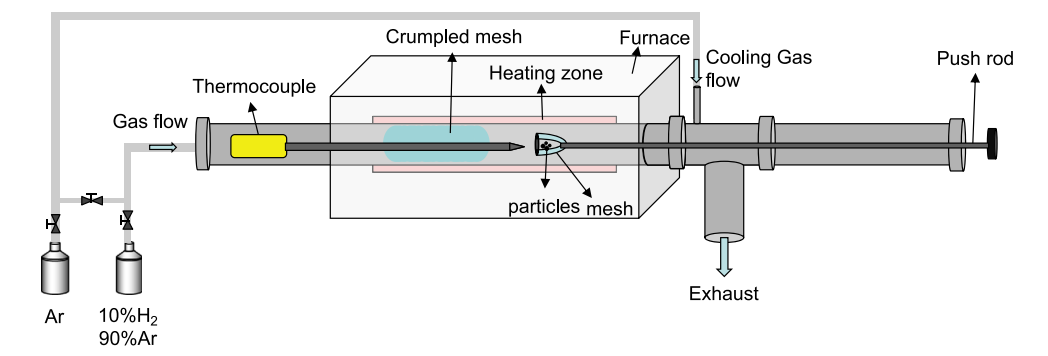


Fig. 2. Experimental setup for the thermal iron-ore reduction using hot gas heated inside an electric furnace.

measured by the spectrometer. The wavelength-dependent sensitivity of the optical system consisting of fiber and spectrometer was corrected for using the spectrum of a calibration light source (Ocean Optics HL-3P-INT-CAL). During the reduction process, light was recorded with a time resolution of one second, which allowed for a sufficient signal-to-noise ratio for an accurate temperature determination. A median filter was applied to the measured spectra to remove the minor contribution of plasma line emission. The measured spectra were fitted to Planck's law to obtain the black-body temperature in the wavelength range of 500 nm to 1100 nm.

For the furnace-based reduction, a K-type thermocouple with ungrounded junction and 1.6 mm wire diameter (response time $\sim\!\!5\,\mathrm{s}$ [39]) was used to measure the gas temperature, as shown in Fig. 2. The thermocouple was surrounded by a ceramic tube, resting on the bottom of the furnace. The low thermal conductivity of the ceramic ensured that the thermocouple was measuring the gas temperature instead of that of the furnace walls. Only the tip of the thermocouple was exposed, to ensure that the measurement position was well-defined and located close to the particle position during the reduction. After reaching a steady state, the temperature reported by the thermocouple was always in good agreement with the set-point temperature of the furnace.

It would have been preferable to utilize the same method of temperature measurement in both the furnace and the plasma reactor. However, geometrical constraints made employing the optical method inside the furnace impossible, while the thermocouple measurements proved too slow for the rapid MW plasma-based reduction process. To ensure that both methods deliver comparable results, we performed a comparison measurement, employing both methods simultaneously in a 60 s long plasma process. When the thermocouple was touching the mesh and sufficient time was allowed for the thermocouple to heat up, the methods agreed to within 1%.

2.4. Quantitative XRD analysis

Treated samples were characterized through X-ray diffraction (XRD). Each sample was crushed and mixed thoroughly to form a homogeneous mixture prior to the analysis. The sample was characterized at multiple locations and an average pattern was analyzed using the Reference Intensity Ratio (RIR) method to calculate the reduction percentage and weight percentage of different phases present in the sample. RIR is an instrument independent constant, specific to the material and the reference material, used in XRD for quantitative phase analysis [40]. The weight percentages of different phases are calculated using the following equation

$$X_{\alpha} = \frac{I_{\alpha}}{\text{RIR}_{\alpha}} \left[\sum_{j=1}^{\infty} \frac{I_{j}}{\text{RIR}_{j}} \right]^{-1}$$
 (4)

where X_{α} is the weight percent of the phase α and I_{α} stands for the integrated intensity of the strongest line of phase α . The index j denotes all other phases of the mixture. RIR $_{\alpha}$ is defined as RIR $_{\alpha} = I_{\alpha}/I_{c}$, i. e. the

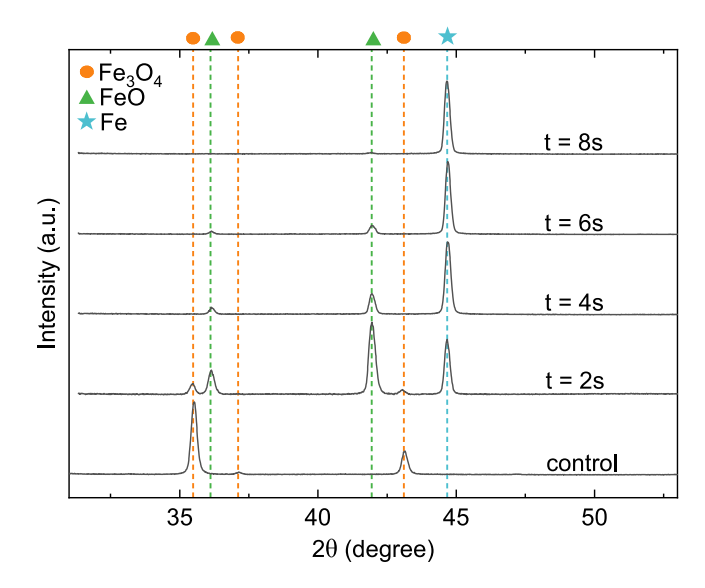


Fig. 3. XRD pattern for magnetite particles treated with the plasma effluents for different times. The color-coded vertical lines indicate peaks belonging to the different iron oxide phases and pure iron.

ratio of the intensity of the strongest peak of the phase α to the strongest peak of the reference material corundum for a 1:1 mixture by weight. The RIR values of magnetite, wüstite, and metallic iron are 5.22, 5.29, and 11.91, respectively. After calculating the weight percentage X_{α} for each phase, the reduction percentage is calculated as

Reduction
$$\% = 100 \frac{\text{calculated mass of oxygen removed}}{\text{calculated mass of oxygen in the sample initially}}$$
(5)

The Powder Diffraction Files (PDF) used were #98-000-0294 (magnetite), #98-001-3836 (wüstite), and #98-000-0259 (metallic iron).

3. Results

3.1. Reduction kinetics of hydrogen microwave plasma

Initially, $10\,\mathrm{mg}$ of magnetite particles were treated with the MW plasma, using different treatment times to study the reduction kinetics. The total gas flow was $45\,\mathrm{slm}$ while the treatment time was varied between $2\,\mathrm{s}$ and $8\,\mathrm{s}$. Fig. 3 shows the XRD pattern of the samples, highlighting the different peaks belonging to $\mathrm{Fe_3O_4}$ (magnetite), FeO (wüstite) and Fe (iron). For the untreated control sample, we exclusively observe $\mathrm{Fe_3O_4}$ peaks, confirming the composition of our magnetite samples. For a treatment time of $2\,\mathrm{s}$, strong FeO and Fe peaks become apparent, demonstrating partial reduction. As the treatment

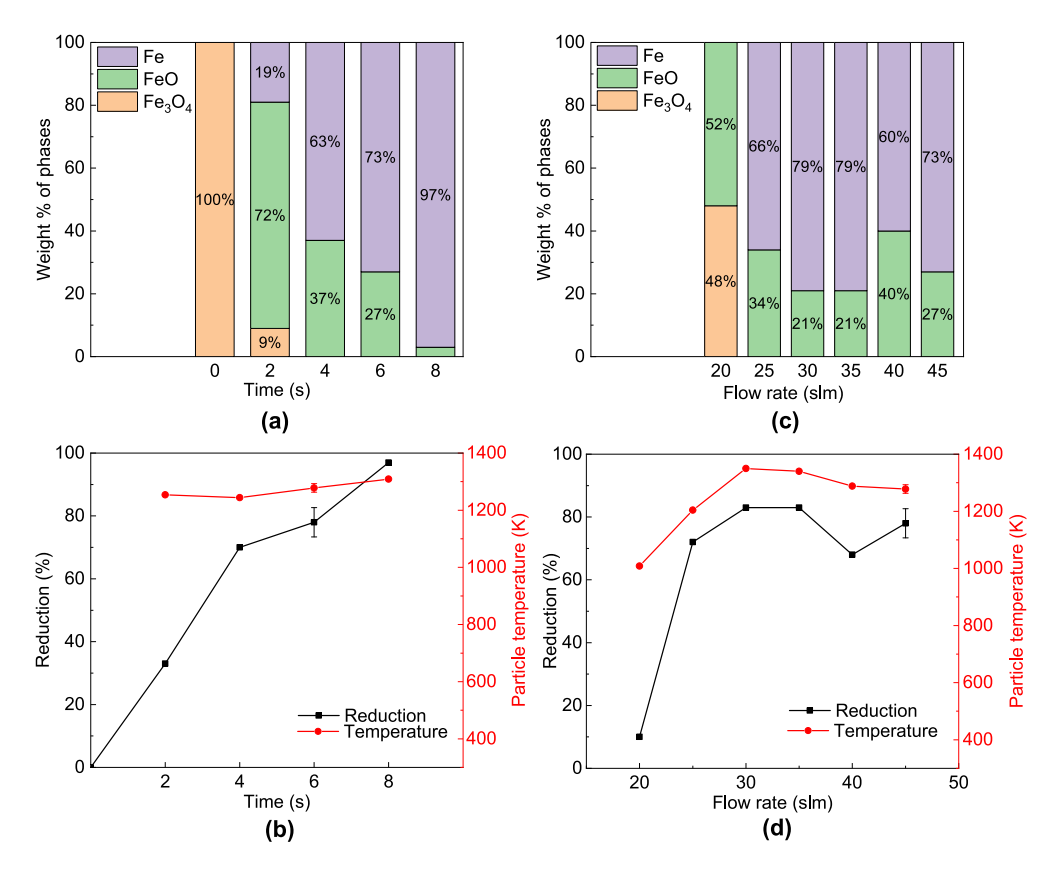


Fig. 4. Plasma-based reduction of 10 mg magnetite particles. (a) and (b) show the composition and percentage reduction, respectively, of the samples treated with the plasma for different times at a gas flow rate of 45 slm. (c) and (d) show the composition and percentage reduction, respectively, of the samples treated with different gas flow rates for a fixed treatment time of 6 s. Selected data points were replicated three times to allow for an error estimation. The error bars indicate ±2 standard error of the mean.

time increases, the FeO peak decreases in its intensity whereas the Fe peak grows, indicating increasing reduction.

This trend is shown more clearly by Fig. 4a which shows the weight percentage of the different phases, calculated from the analysis of Fig. 3. Already after 2 s, the magnetite is mostly reduced to FeO, with further treatment time being necessary to facilitate the reduction from FeO to pure Fe. This result confirms the reduction pathway of Fe₃O₄ \rightarrow FeO \rightarrow Fe, in agreement with the reduction of Fe₃O₄ at temperatures above 840 K [12]. After 8 s treatment the sample is 97% Fe by weight.

Fig. 4b shows the overall reduction percentage (weight or atomic percentage of oxygen removed) for the different treatment times together with the particle temperatures measured during the trials. The particle temperature was almost constant at around $1300\,\mathrm{K}$ for all treatment times. This is in agreement with time-resolved temperature measurements (shown in Figure S3 in supplementary information) which show that due to their low thermal mass, particles and mesh reach their final temperature within our $1\,\mathrm{s}$ time resolution. Thus, the temperature of the particles likely reached a steady state during the experiment, which is the same for all treatment times. For the $6\,\mathrm{s}$ treatment times, the trials were performed three times to allow for an error estimation. The data point shown in the figure is the mean of these trials, while the error bars indicate ± 2 standard error of the mean.

The reduction already reached about 30% after only $2\,s$ treatment time, while nearly complete reduction is reached after $8\,s.$ This reduction speed is comparable to the thermal reduction reported by Choi and Sohn [21] who reduced $30\,\mu m$ magnetite particles suspended in hot hydrogen at $1370\,K.$ A more detailed comparison with prior research is presented below.

Fig. 4c and 4d demonstrate the effect of the gas flow rate on the reduction process and particle temperature at a constant treatment time of 6s. Fig. 4c shows only partial reduction to FeO for low flow rates of 20 slm, while higher flow rates show much stronger reduction

peaking around 85% for 35 slm and then slightly reducing again for larger flows. This trend can be understood to reflect the transport of both heat as well as reactive species from the plasma towards the mesh. Increasing the gas flow will speed up the gas velocity, allowing reactive species like atomic hydrogen to reach the particles before recombining to molecules. An increased gas flow will also result in a higher gas temperature at the particle position, since faster heat transport minimizes the losses to the cool reactor walls. Correspondingly, the particle temperature, shown in Fig. 4d increases with the gas flow to about 1350 K at 30 slm. Even larger gas flows then lower the temperature, presumably because these high gas flows now begin to lower the temperature inside the plasma, as the energy input per gas molecule is lowered. These two competing processes cause the peak in particle temperature and reduction between 30 slm to 35 slm.

Fig. 5a shows a representative SEM (scanning electron microscopy) image of an untreated (before) and an almost fully reduced sample (after), obtained after a treatment time of 8 s at a gas flow rate of 45 slm. The untreated magnetite samples are composed of aggregates, formed from small grains, ranging from hundreds of nm to several μm . Upon reduction, they undergo a large morphological change. The reduced sample shown in Fig. 5a is highly porous with whisker-like structures. The formation of whiskers is a common phenomenon observed when reducing iron ore with hydrogen [41,42]. Thus, the hydrogen plasma effluent treatment is observed to cause the same morphological changes as observed with hot hydrogen gas.

Fig. 5b shows the EDS (energy dispersive X-ray spectrometry) elemental mapping of the sample performed with SEM. The elemental analysis shows pure elemental iron in green, oxygen in blue, and carbon in red, where the carbon results from a carbon coating, deposited to ensure the required conductivity of the sample. The elemental mapping shows the particle surface to consist almost entirely of Fe. Notably, only very little remaining oxygen can be observed in the image,

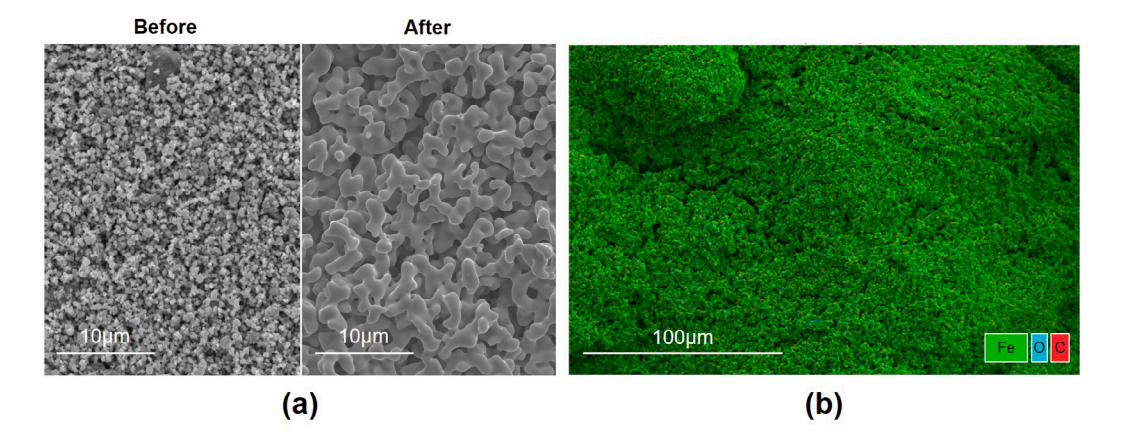


Fig. 5. (a) SEM micrographs of particles before and after plasma treatment. (b) EDS elemental mapping of the 97% reduced sample, obtained after a treatment time of 8s at a gas flow rate of 45 slm.

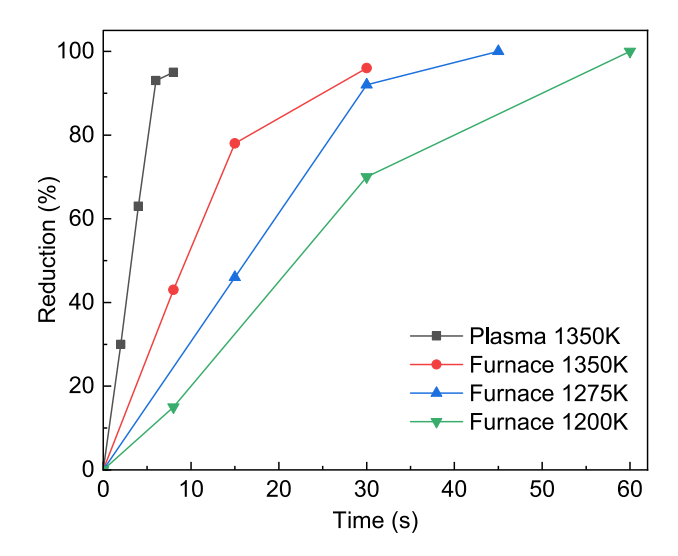


Fig. 6. Magnetite reduction using a hot argon-hydrogen (90:10 volume %) gas mixture inside the electric furnace at gas temperatures of $1200\,\mathrm{K}$, $1275\,\mathrm{K}$ and $1350\,\mathrm{K}$. For comparison, the figure shows the plasma-based reduction at $35\,\mathrm{slm}$ gas flow, with particles reaching a temperature of $1350\,\mathrm{K}$.

corresponding to an atomic percentage of 1.9%. This confirms the XRD results which indicate a weight percentage of 97% iron for the above-mentioned sample.

3.2. Comparison between MW plasma and thermal reduction

To investigate the influence of reactive plasma species, the MW plasma reduction was compared to a fully thermal reduction. Samples of $10\,\mathrm{mg}$ of particles were treated at different temperature with hot argon–hydrogen (90:10) flowing at 35 slm for varying times from 8 s to 60 s and their reduction measured with XRD. The results of this study are shown in Fig. 6, together with the MW plasma reduction, performed at a gas flow rate of 35 slm.

For all treatment conditions shown in Fig. 6, the measured reduction increases with treatment time, as expected. For the three thermal reductions performed in the furnace, the speed of reduction increases with temperature. Interpolating between the data points, we can see that it takes about $50\,\mathrm{s}$ to reach 95% reduction for $1200\,\mathrm{K}$. For $1275\,\mathrm{K}$ and $1350\,\mathrm{K}$, this level of reduction is already reached after about $35\,\mathrm{s}$ and $30\,\mathrm{s}$, respectively. Due to the temperature limitations of the furnace, trials at temperatures higher than $1350\,\mathrm{K}$ were not conducted.

For the initial 70% reduction, the reduction rate (weight % of oxygen removed per second) is almost constant, as can be deduced from the linear trend visible in Fig. 6. For the furnace trials at 1200 K, 1275 K, and 1350 K, we find values of around 2.2, 3 and 5 %/s, respectively. The increase in reduction rate is expected due to the higher reaction and diffusion rates at higher temperatures. Using the Arrhenius plot (figure S1 in the supplementary information), $\ln(\text{reduction rate})$ vs T^{-1} , the apparent activation energy for the furnace trials is estimated to be around 70 kJ mol⁻¹. In comparison, the plasma-based process has a relative reduction rate of 15 %/s, about three times higher than the purely thermal reduction performed at the same temperature. This speed advantage becomes even more pronounced if we instead consider the time needed to reach 95% reduction. Since the thermal reduction performed in the electric furnace slows down at higher reduction percentages, the plasma is about four times faster in reaching 95% reduction, needing only 8s instead of 30s needed for the thermal reduction. Assuming a 3 times faster reduction with plasma and the same reaction kinetics law for furnace and plasma reduction, the apparent activation energy for plasma trial can be estimated as 60 kJ mol⁻¹, indicating a 15% decrease in activation energy due to plasma species such as atomic hydrogen.

It should be noted that the two setups, used for either the thermal or the plasma-based reduction, are not perfectly identical in how the particles are inserted into the heating zone. In the plasma, the mesh onto which the particles are placed covers the entire reactor crosssection, forcing the gas flow through the mesh and the particle layer. In the furnace, however, part of the gas can flow around the cup formed by the mesh, thus potentially lowering the hydrogen concentration at the particle position as hydrogen is used up by the reduction process and less quickly replenished by the gas flow. To estimate whether this effect could influence the reduction rate, we consider the diffusion time scales of molecular hydrogen in argon, with a binary diffusion coefficient of about $D = 1 \times 10^{-3} \,\mathrm{m}^2/\mathrm{s}$ at 1275 K [43] and with a diffusion length of $L = d/\pi$ where $d = 1.5 \,\mathrm{cm}$ is the depth of the cup in which the particles are placed. The diffusion time scale can then be estimated to $\tau = L^2/D \approx 30 \,\mathrm{ms}$, which is much faster than the reduction. Thus, diffusion could compensate for the loss of hydrogen molecules due to the reduction process, even if none of the gas passed through the particles. The same estimate can be made for the diffusion time scale needed for water vapor formed in the reduction process to diffuse out of the cup. The binary diffusion coefficient of water vapor in Ar is calculated using the Chapman-Enskog theory [44] as $3.4 \times 10^{-4} \,\mathrm{m}^2 \,\mathrm{s}^{-1}$ at 1275 K. The diffusion time scale is estimated to be about 70 ms, indicating that diffusion is fast enough to avoid any significant water concentration around the particles to hamper reduction. Hence, the differences between the two setups should not affect the obtained reduction rates even in the worst-case scenario when the gas is fully bypassing the mesh cup.

We propose that the faster plasma reduction is based on the decrease in the activation energy due to the presence of reactive plasma species [25]. However, this begs the question of which reactive species have a sufficiently long lifetime to reach the magnetite particles at a distance of roughly 140 mm downstream of the plasma.

The MW plasma creates a multitude of excited and reactive species. However, only a few of these have sufficiently long lifetimes in an atmospheric pressure environment to reach the magnetite particles. Assuming a gas temperature of around 2000 K in the plasma effluent, the species carried with the gas flow will need about 14 ms to reach the particle position. This is considerably longer than the lifetime of many of the excited species.

For instance, electronically excited states of hydrogen atoms have radiative lifetimes of at most a few μs [45], which is further reduced by heavy particle collisions at atmospheric pressure. Similarly, based on the recombination rates for the dominant ionic species (H₃⁺ or ArH⁺) [46,47] we expect charge carries to have recombined below densities of $1 \times 10^{15} \, \mathrm{m}^{-3}$ before they reach the particles (compare section 2 in the SI). This corresponds to a flux of about $4 \times 10^{12} \, \mathrm{ions/s}$ onto the particles, which is negligible compared to the $2.6 \times 10^{19} \, \mathrm{Fe_3O_4}$ molecules contained within our $10 \, \mathrm{mg}$ sample.

Therefore, the species most likely responsible for the increased reduction rate of the plasma process seems to be atomic hydrogen, created inside the plasma by the dissociation of hydrogen molecules. Thus, we estimate the amount of atomic hydrogen reaching the particles using three-body volume recombination and radial loss to the walls. The change in atomic hydrogen density $n_{\rm H}$ can be written

$$\frac{\partial n_{\rm H}}{\partial t} = -k_r n_g n_{\rm H}^2 - \frac{D}{\Lambda^2} n_{\rm H} \tag{6}$$

with the time t, the gas density n_g , the volume recombination rate coefficient k_r , the binary (H–Ar) diffusion coefficient D and characteristic radial diffusion length $\Lambda = R/2.4$ [48].

The equation is solved numerically over a time of 14 ms, after which the gas flow should have reached the iron ore particles. We assume a constant gas temperature of 2000 K and H–Ar binary diffusion of $D=3.8\times 10^{-3}~\text{m}^2/\text{s}$ [49]. The gas density is calculated to $n_g=3.6\times 10^{24}~\text{m}^{-3}$ using the ideal gas law. For the reaction rate coefficient, we use the value of $k_r=5\times 10^{-45}~\text{m}^6/\text{s}$, as measured by Halstead and Jenkins [50] in a flame experiment performed at 1900 K. This value of k_r was measured for pure argon, instead of an argon–hydrogen mixture as we use in our experiment. However, the rate coefficient for recombination with H_2 as the reaction partner is similar to the one for argon [51], so that the reaction rate coefficient for our argon–hydrogen gas mixture should be close to the one of pure argon.

Since the dissociation degree inside the plasma is unknown, we estimate a lower and an upper limit assuming either 10% or full dissociation, respectively. Additionally, wall losses will be neglected for the upper limit, effectively setting D=0.

The upper and lower limits of the atomic hydrogen density as a function of time are shown as figure S2 in the supplementary information, which also contains more details about the calculation. For the upper limit, we calculated the atomic hydrogen density around the particles to $n_{\rm H}=4\times10^{21}\,{\rm m}^{-3}$, while we find a value of $n_{\rm H}=8\times10^{20}\,{\rm m}^{-3}$ for the lower limit. This corresponds to the atomic hydrogen flux of 1.5×10^{19} atoms/s to 3×10^{18} atoms/s. For a complete reduction of 10 mg magnetite particles in 10 s with H atoms, a flux of 2×10^{19} atoms/s is required. This indicates that the calculated H atom flux to the particles is 14% to 73% of the flux required for complete reduction with H atoms alone. As pointed out by Sabat and Murphy [25], even about 2% atomic hydrogen together with 8% vibrationally excited H2 in hydrogen can decrease the activation energy needed for the reduction process by half. Thus, it seems likely that the atomic hydrogen created by the plasma can explain the lower reduction times observed when compared to the furnace reduction.

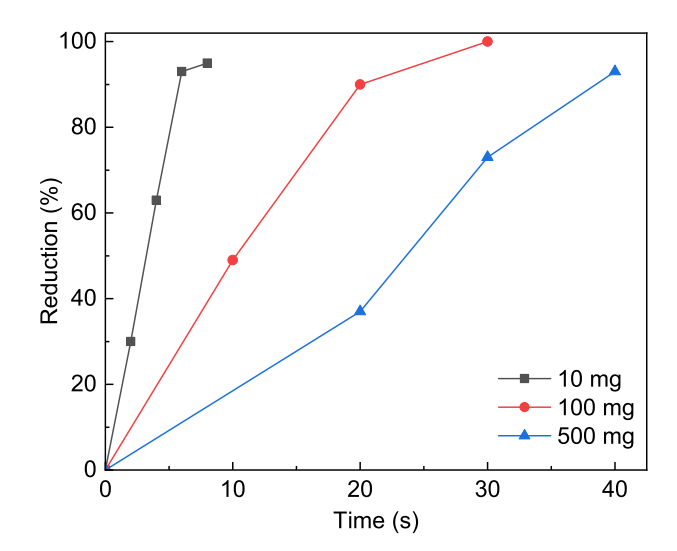


Fig. 7. Plasma-based magnetite reduction for different particle mass loads at a constant gas flow rate of 35 slm.

3.3. Mass scaling and energy efficiency

Having demonstrated that hydrogen plasma can rapidly reduce small amounts of magnetite, we now assess the impact of increasing mass load on the reduction of magnetite particles. To this end, the MW plasma reduction was conducted with $10\,\mathrm{mg}$, $100\,\mathrm{mg}$, and $500\,\mathrm{mg}$ of magnetite particles placed on the mesh. Fig. 7 shows the reduction of particles as a function of the treatment time at three different mass loads and a constant gas flow rate of $35\,\mathrm{slm}$. The particle temperature reduced slightly with increasing treatment time, but did otherwise not vary significantly for the different mass loads and was always between $1350\,\mathrm{K}$ and $1270\,\mathrm{K}$, as shown in figure S3 in the supplementary information.

The time needed to reduce the magnetite particles increases with the mass load. The 10 mg sample needed only 6s to reach a reduction above 90%, while 20 s and 40 s were needed for the 100 mg and 500 mg samples, respectively. The increased reduction time at higher mass load seems to be caused by hydrogen transport limitations to the particles positioned at the bottom of the particle pile. At a mass load of 10 mg, particles form only a few layers on top of the mesh, whereas at 100 mg and 500 mg, the particle pile reaches a depth of up to 1 mm and 4 mm, respectively. Consequently, at higher mass loads the top of the particle pile was observed to be reduced first, with particles located at the bottom only showing evidence of reduction after much longer treatment times. This is indicated by the color change of the material from initially black towards metallic silver after reduction. For the 500 mg sample and a treatment time of 20 s, we also collected samples from the top and the bottom of the pile, to confirm this finding with XRD analysis, which revealed that the particles collected from the top of the pile were 65% reduced whereas the bottom particle showed only 6% reduction (compare figure S4 in the SI). It should be noted that the results shown in Fig. 7 were obtained after thoroughly mixing the samples after the treatment, thus showing average reduction values.

As Fig. 7 demonstrates the reduction rate for $10 \,\mathrm{mg}$, $100 \,\mathrm{mg}$, and $500 \,\mathrm{mg}$ trials for the initial 90% reduction are around 15.5, 4.5, and $2.3 \,\%/\mathrm{s}$ respectively showing a decrease in reduction rate with the increasing mass load. However, the conversion of hydrogen to water is improving with the increased mass load. The rate of hydrogen conversion increases from $3 \,\mathrm{mg\,min^{-1}}$ for $10 \,\mathrm{mg}$ trials to $9 \,\mathrm{mg\,min^{-1}}$ for $100 \,\mathrm{mg}$ and $24 \,\mathrm{mg\,min^{-1}}$ for $500 \,\mathrm{mg}$ trials indicating an improved hydrogen utilization at higher mass loads. Even for the $500 \,\mathrm{mg}$ trial, only about 8% of the total hydrogen flow is utilized for the reduction

process. Hence, on increasing the mass load of the magnetite particles, more hydrogen is now utilized for the reduction process.

Increasing the mass load 10 and 50 times increases the required time for reduction only by about a factor of 4 and 7, respectively. This indicates an improvement in energy efficiency for 500 mg trials versus 10 mg trials by about an order of magnitude. The reduction of 500 mg of magnetite to 92% Fe within 40 s corresponds to an electrical energy consumption of about 170 GJ t⁻¹ of Fe produced. Additionally, hydrogen is only consumed for the magnetite reduction in the MW plasma-based reduction and not for combustion. Hence, the hydrogen consumption of the process can be as small as $48 \,\mathrm{kg} \,\mathrm{t}^{-1}$ of Fe produced if the exhaust hydrogen is captured and reused. Similarly, the consumption of Ar is negligible if the exhaust gas is reused. Assuming an energy cost of around 170 MJ kg⁻¹ of green hydrogen using current commercial electrolysis cells [52], this will add an additional energy cost of around 8 GJ t-1 of Fe produced. In comparison, the energy consumption of conventional ironmaking, including blast furnace, coking, and pelletization, is around 16 GJ t⁻¹ of Fe [53].

Thus, our current lab-scale MW plasma consumes about 10 times more energy than the conventional process, when only considering the electrical power needed for the reduction. However, achieving the gas temperature just above the mesh of $1350\,\mathrm{K}$ requires only a heating power of about $600\,\mathrm{W}$, of the totally supplied $1700\,\mathrm{W}$. Thus, about 65% of the energy is lost to the reactor walls. If this energy loss is avoided, the setup has the potential to achieve an energy consumption of about $60\,\mathrm{GJ}\,\mathrm{t}^{-1}$ of Fe produced, only 4 times more than the conventional route. A system recovering the heat lost as the hot gas exits the reactor can further improve the energy efficiency of the process.

The results presented in this work were obtained for samples with a maximum mass of 500 mg. However, given the favorable increase in treatment time with mass loading, demonstrated in Fig. 7, it seems that even higher mass loads might lead to better energy efficiencies. A scale-up of the current technology could involve a combination of the following strategies: (i) operation with pure hydrogen to achieve faster reduction kinetics; (ii) higher power microwave generators operating at lower frequency to enable larger plasma volumes, (iii) improved particle delivery to achieve higher mass loads and better particleplasma contact, (iv) heat recovery to improve the energy efficiency. Different from the incumbent blast furnace technology, the microwave plasma technology will likely be modular and scale-up will involve parallelization, which is attractive for its compatibility with intermittent renewable electricity. Techno-economic studies, which are beyond the scope of the current report, are needed to evaluate these different strategies.

Additionally, one of the biggest questions for the application of the current work for future industrial applications is the cost-effective production of green hydrogen. To this end, a considerable amount of research is currently devoted to optimizing the cost and CO_2 emission of hydrogen production, exploring techniques like electrolysis, photocatalytic water splitting, biological hydrogen production, and steam reforming of ethanol [54–57]. Currently, water electrolysis is the dominant green hydrogen production technique and costs around \$4.85 kg^{-1} of green $\mathrm{H_2}$ [58]. However, the cost is estimated to decline to \$2 kg^{-1} by 2030 [58]. Thus, the global demand for reducing carbon emissions is driving research and innovations in hydrogen production to enable the application of green hydrogen in industrial processes in the near future.

3.4. Reduction of hematite and natural iron ore

In addition to the magnetite particles investigated so far, natural iron ore usually contains different oxidation states of iron, as well as impurities, such as ${\rm SiO_2}$, MgO, and moisture. To first investigate the influence of the oxidation state on the reduction process, 500 mg of hematite (Fe₂O₃) particles were reduced with a gas flow rate of 35 slm. The utilized hematite particles had the same size (<5 μ m) and purity

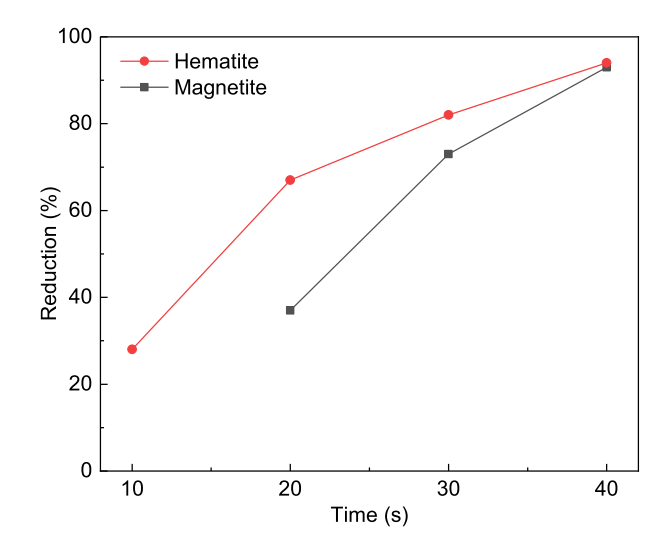


Fig. 8. Comparison of the reduction of 500~mg hematite and magnetite particles at a gas flow rate of 35~slm.

as the magnetite (Fe₃O₄) particles. Since hematite is expected to first reduce to magnetite, with the reduction proceeding from there (see reaction (2)), one might suspect a slower reduction of the hematite particles. However, Fig. 8 demonstrates the opposite. During the initial stages of reduction, the reduction rate for hematite particles is larger than for magnetite particles. This agrees with other studies, often reporting slower magnetite reduction due to its non-porous structure leading to the formation of a dense layer of iron on the surface during the process [59]. However, only minor differences were found for our small particles, since both oxidation states require the same 40 s to reach 90% reduction. The higher initial reduction rate for hematite might be caused by the relative ease of reducing hematite to magnetite. In contrast, the time needed to reach complete reduction is mostly determined by the conversion from wüstite to Fe as the rate-limiting step, leading to comparable times to achieve 90% reduction for both oxidation states.

To confirm the suitability of the process for the reduction of industrial iron ore, we tested natural black iron ore powder containing 2.9% SiO₂, 1% moisture, 0.2% MgO, and 0.2% Ca. The powder was sieved to size $<37 \,\mu m$ to remove the bigger chunks and treated with the plasma effluent under typical conditions. For 10 mg of natural iron ore, 89% reduction was reached after 30 s. Thus, the reduction of the <37 µm natural iron ore particles took about five times longer than the reduction of the $<5\,\mu m$ magnetite particles. Both the larger particle size and as well as the impurity content in the natural iron ore may slow the reduction. It is likely that the small particle size (\sim 5 μ m) is more suitable for the reduction process. Since the steel industry already uses rotating mills to reduce iron ore to ${\sim}50\,\mu m$ particles during the iron ore beneficiation process, achieving a particle size of \sim 5 μm would require an increase in the milling time. For instance, Hanumanthappa et al. [60] showed that ball milling 150 µm iron ore particles for 13 min produced a particle size distribution with 55% of particles having a size of less than 10 μm. Increasing the milling time will increase the energy cost of the process. However, the energy consumption of the milling process (4 MJ t⁻¹ of iron ore produced [61]) is negligible in comparison to major energy-consuming processes like blast furnaces (~16 GJ t⁻¹ of Fe [62]) and therefore not a major concern. However, further research is needed to analyze the role of particle size and impurities on the reduction and will be carried out in future work.

3.5. Comparison to other processes

The process presented in this work is now compared to similar, mostly laboratory scale technologies reported in the literature using

Table 1
Comparison of some lab-scale iron ore reduction techniques reported in the literature using hydrogen as a reducing agent. The listed times corresponds to a reduction to about 90% (88% to 96%).

Work	Ore	Reduction process	Gas composition (%)	Size (um)	T (K)	Initial mass (mg)	Time (s)	Reduction rate (%/s)
This	Fe ₃ O ₄	Plasma effluent	10H ₂ -90Ar	5	1350	10	6	15.5
This	Fe_3O_4	Plasma effluent	10H ₂ -90Ar	5	1350	500	40	2.3
This	Fe_3O_4	Electric Furnace	10H ₂ -90Ar	5	1350	10	30	3.2
[63]	Fe_3O_4	Drop tube (5.6 cm diameter, 193 cm height)	23H ₂ -77N ₂	22.5	1600	7 ^a	2.6 ^b	34.0
[63]	Fe_3O_4	Drop tube (5.6 cm diam, 193 cm height)	$71H_2-29N_2$	35	1410	11.6 ^a	5.8 ^b	15.8
[8]	Fe_3O_4	Drop tube (0.8 m diam, 2.1 m height)	H_2 - CH_4 - O_2	<100	1620	25 200 ^a	14.4 ^b	6.2
[64]	Fe_3O_4	Packed bed (8 mm diam)	50H ₂ -50Ar	0.25	820	1500	490	0.19
[65]	Fe_2O_3	Fluidized bed (68 mm bed diam)	$65H_2$ - $35N_2$	250-500	1070	400 000	1500	0.06
[66]	Fe_xO	Fluidized bed (50 mm bed diam, 2ft long)	H_2	210–1190	870	400 000	300	0.3
[23]	Fe_2O_3	Vibrating fluidized bed with solar irradiation	H_2	10–15	770	500 000	2700	0.03
[67]	Fe_2O_3	Isothermal reduction of porous compacts (12.3 mm diam. 13.5 mm height, 35% porosity)	H_2	0.6	1370	4000	320	0.3
[68]	Fe_3O_4	Furnace reduction of fines (8 mm diam, 5 mm height, 27% porosity)	H_2	106–125	1270	200	600	0.16
[69]	Fe_3O_4	Furnace reduction of fines (11 mm diam, 3 mm height)	H_2	1.5	670	50	200	0.47
[70]	Fe_3O_4	Isothermal reduction of single crystal	H_2	4000 × 4000 × 8000	1370	1000	4530	0.02
[71]	Fe_3O_4 and Fe_2O_3	Blast Furnace simulator using Sintered pellet (95 mm diam)	H ₂ -CO	12 500- 16 000	1270	100 000	7200	0.01
[72]	Fe_2O_3	Thermal plasma arc	40H ₂ -60Ar	10-1000	2600	100 000	2000	0.05
[36]	85% Fe ₂ O ₃	Low pressure plasma reduction of compacted pellet	H_2	40 000	1070	2570	1800	0.05

^aIndicates mg of particles reduced obtained by multiplying particle feed rate with residence time.

hydrogen or hydrogen gas mixtures as the reduction agent. Since the work in this field started as early as the 1960s or before, there is a vast number of publications available, only a small selection of which is discussed here. With the data selected in Table 1 we try to report a representative value of the typical reduction rate observed with the respective technique.

However, it should be noted that the different experiments vary widely in regards to operating parameters (like temperature, pressure, gas composition) and properties of particles (like grain size, mineralogy, porosity, specific surface area and tortuosity). Since all of these factors influence the reduction [59], and values like the particle porosity are usually not reported, it is not possible to calculate a single common value to describe the merit of the reduction process. Thus, the comparison in Table 1 should be used with caution and is only given to provide the reader an idea of typical reduction rates and operating parameters used in different processes with hydrogen as a reducing agent.

Table 1 lists the type of reactor and the various operating parameters used in the reduction processes. The size column lists the particle size in case of a reduction of iron ore fines or otherwise shows the ingot or pellet size. The reduction rate was calculated from the reduction percentage and the processing time reported in the respective experiments. The listed processing times corresponds to the time needed to achieve about 90% reduction (88% to 96%).

For the different processes, the calculated relative reduction rate varies from $0.01\,\%/s$ to $34\,\%/s$. The fastest reduction rate is observed for the in-flight reduction of iron ore concentrates, developed at the University of Utah [63]. In their drop tube reactor, where the gas is heated electrically, a relative reduction rate as high as $34\,\%/s$ was observed. The reason for this high reduction rate is the high temperature of $1600\,\mathrm{K}$ and the good contact between the dropping particles and the gas. At a lower temperature of $1410\,\mathrm{K}$, the relative reduction rate in the same experiment dropped to $15.8\,\%/s$, virtually the same value as for the reduction of $10\,\mathrm{mg}$ magnetite using our MW plasma $(15.5\,\%/s)$. However, our process uses a lower concentration of hydrogen to achieve this reduction rate.

In the pilot plant developed at the University of Utah, a scaled-up version of the drop tube reactor was used to achieve $6\,\%/s$ at $1620\,\mathrm{K}$. Here, the heat was generated using the partial combustion of methane, hydrogen, and oxygen. The combustion produces water vapor which reduces the thermodynamic driving force for the reduction [59], which explains the lower reduction rate compared to the electrically heated lab scale prototype [63]. The combustion of methane will also necessarily produce CO_2 as a by-product, diminishing the advantage compared to fully electric operation.

In their packed bed reactor, Baolin et al. achieved a relative reduction rate of $0.19\,\%/s$ when reducing $1500\,\mathrm{mg}$ of magnetite particles [64]. This relative reduction rate is about an order of magnitude lower than the rate reported here for the reduction of $500\,\mathrm{mg}$ particles using the MW plasma. The reason for this difference is likely the lower temperatures at which the packed bed reactor was operated and the smaller cross-section, implying a larger height of the particle stack and, thus, increased difficulty of hydrogen reaching the lower parts of the bed

This drawback can be overcome by fluidized bed reactors [65,66], which offer good contact between particles and the reducing gas as well as the ability to handle a large amount of particles. However, these reactors cannot use high temperatures to achieve better reduction kinetics. This is due to the increased softness and adhesion of the highly active iron formed at these temperatures, which leads to agglomeration and sticking of particles, eventually leading to defluidization [73]. Thus, typical temperatures for fluidized bed reactors were reported to lie between $800\,\mathrm{K}$ and $1100\,\mathrm{K}$, leading to comparatively low reduction rates between $0.06\,\%/\mathrm{s}$ and $0.3\,\%/\mathrm{s}$.

Li et al. [23] used a vibrating fluidized bed to reduce hematite particles ($10\,\mu m$ to $15\,\mu m$) with solar-heated hydrogen gas at $770\,K$, overcoming the need for combustion or electrical heating for the process heat. However, since the process is aimed to operate at low temperatures, the reduction required long times of around 50 min with a reduction rate of around $0.03\,\%/s$.

bIndicate residence time of particles in seconds.

Much higher temperatures can be achieved using thermal arc hydrogen plasmas. These processes can produce interface temperatures as high as $3000\,\mathrm{K}$ and reactive hydrogen species such as hydrogen atoms/ions to melt the iron ore and enable fast reduction kinetics [25]. Badr showed in their lab scale experiments the reduction of $100\,\mathrm{g}$ of iron ore with an 8 kW DC transferred-arc reactor [72]. Typical reduction rates observed were $0.05\,\%/\mathrm{s}$ at plasma-melt interface temperatures between $2270\,\mathrm{K}$ and $2870\,\mathrm{K}$.

Rajput et al. used a low-pressure plasma, operating at 1.3×10^4 Pa and $1070\,\mathrm{K}$, to reduce hematite pellets at a reduction rate of $0.05\,\%/s$. The observed low reduction rates are due to the low temperature and pressure of hydrogen used in this study along with the use of big pellets (40 mm) where the process is mass transfer limited.

In comparison to the literature, the reduction rates observed in this work are quite promising, given the moderate temperature (1350 K) and hydrogen partial pressure (0.1 atm). Under similar conditions, our reported reduction rates are on-par with the fastest reduction we could find reported in the literature. Heating hydrogen with a microwave plasma source has the potential to be entirely carbon-free when utilizing green hydrogen and renewable electricity. The process is also compatible with the intermittent nature of renewable energy due to it's low thermal inertia and virtually no heat-up time.

However, the comparison to the literature also underlines the importance of heat and good contact between particles and the reducing agent. In this regard, in-flight reduction seems the ideal approach to optimize the reduction rate. But this will require a considerable increase in particle residence time which is currently only on the order of $10\,\mathrm{ms}$.

4. Conclusion

A novel method was introduced to reduce iron ore using an atmospheric pressure hydrogen plasma. A fully electrified microwave setup is used to ignite plasma in an argon–hydrogen gas mixture. The gas flow transports heat and reactive plasma species to the magnetite particles placed below, causing their reduction. The plasma process reduced $10\,\mathrm{mg}$ of magnetite particles to $>\!90\,\%$ metallization in 6 s. Favorable scaling to higher mass loads was demonstrated, with a 50 times increase in particle mass only resulting in an increase of reduction time by a factor of 7.

The microwave plasma reduction was compared to a thermal reduction, heating the argon–hydrogen mixture using an electric furnace. Under comparable temperatures, the plasma-based reduction is three to four times faster than the thermal reduction inside a furnace, which may be due to atomic hydrogen created by the plasma.

The proposed technology has the potential to be a zero-carbon process when using green hydrogen and renewable electric energy. If heat losses can be minimized, we project that the current lab-scale prototype can approach the energy efficiency of the conventional blast furnace to within a factor of four. In-flight reduction of the iron ore powders may lead to an additional speed up of the reduction. However, the technology requires further development to enable scale-up, energy efficiency, and economic hydrogen production for an industrial application.

Declaration of competing interest

The authors declare the following financial interests/personal relationships which may be considered as potential competing interests: A United States patent application has been filed by the University of Minnesota that lists Bruggeman, Held, Kortshagen, Kumar and Xiong as inventors.

Data availability

Data will be made available on request.

Acknowledgments

We thank Dr. Wei Xiao for his contribution in designing and building the MW plasma source. We thank Benjamin Yeh (University of Minnesota) and Dr. Aditya Bhan (University of Minnesota) for their help in conducting BET surface area analysis.

This work was supported by the University of Minnesota under the Ronald L. and Janet A. Christenson Chair in Renewable Energy. Parts of this work were carried out in the Characterization Facility, University of Minnesota, which receives partial support from the U.S. National Science Foundation through the MRSEC program (Award Number DMR-2011401) and the NNCI program (Award Number ECCS-2025124).

Appendix A. Supplementary data

Supplementary material related to this article can be found online at https://doi.org/10.1016/j.cej.2023.145025.

References

- Worldsteel association, Climate Change and the Production of Iron and Steel Transforming Steel Production, Tech. Rep., WSA, 2021, URL https://worldsteel. org/wp-content/uploads/Climate-policy-paper-2021.pdf.
- [2] P. Jin, Z. Jiang, C. Bao, S. Hao, X. Zhang, The energy consumption and carbon emission of the integrated steel mill with oxygen blast furnace, Resour. Conserv. Recv. 117 (2017) 58–65, http://dx.doi.org/10.1016/j.resconrec.2015.07.008.
- [3] International Energy Agency, Net Zero by 2050: A Roadmap for the Global Energy Sector, Tech. Rep., IEA, 2021, p. 224, URL https://www.iea.org/reports/ net-zero-by-2050.
- [4] S.H. Yi, M.E. Choi, D.H. Kim, C.K. Ko, W.I. Park, S.Y. Kim, FINEX® as an environmentally sustainable ironmaking process, Ironmak. Steelmak. 46 (7) (2019) 625–631, http://dx.doi.org/10.1080/03019233.2019.1641682.
- [5] D. Leeson, N. Mac Dowell, N. Shah, C. Petit, P.S. Fennell, A techno-economic analysis and systematic review of carbon capture and storage (CCS) applied to the iron and steel, cement, oil refining and pulp and paper industries, as well as other high purity sources, Int. J. Greenh. Gas Control 61 (2017) 71–84, http://dx.doi.org/10.1016/j.ijggc.2017.03.020.
- [6] M. Pei, M. Petäjäniemi, A. Regnell, O. Wijk, Toward a fossil free future with hybrit: Development of iron and steelmaking technology in Sweden and Finland, Metals 10 (7) (2020) 1–11, http://dx.doi.org/10.3390/met10070972.
- [7] M.N. Seftejani, J. Schenk, Thermodynamic of liquid iron ore reduction by hydrogen thermal plasma, Metals 8 (12) (2018) 1051, http://dx.doi.org/10. 3390/met8121051.
- [8] H.Y. Sohn, D.Q. Fan, A. Abdelghany, Design of novel flash ironmaking reactors for greatly reduced energy consumption and CO2 emissions, Metals 11 (2) (2021) 1–28, http://dx.doi.org/10.3390/met11020332.
- [9] J. Wiencke, H. Lavelaine, P.J. Panteix, C. Petitjean, C. Rapin, Electrolysis of iron in a molten oxide electrolyte, J. Appl. Electrochem. 48 (1) (2018) 115–126, http://dx.doi.org/10.1007/s10800-017-1143-5.
- [10] D.V. Lopes, M.J. Quina, J.R. Frade, A.V. Kovalevsky, Prospects and challenges of the electrochemical reduction of iron oxides in alkaline media for steel production, Front. Mater. 9 (2022) 1010156, http://dx.doi.org/10.3389/fmats. 2022 1010156
- [11] X. Zou, S. Gu, X. Lu, X. Xie, C. Lu, Z. Zhou, W. Ding, Electroreduction of iron (III) oxide pellets to iron in alkaline media: a typical shrinking-core reaction process, Metall. Mater. Trans. B 46 (2015) 1262–1274, http://dx.doi.org/10. 1007/s11663-015-0336-8
- [12] A. Heidari, N. Niknahad, M. Iljana, T. Fabritius, A review on the kinetics of iron ore reduction by hydrogen, Materials 14 (24) (2021) 7540, http://dx.doi.org/ 10.3390/ma14247540.
- [13] T.J. Park, J.H. Lee, D.G. Kim, H. Kim, Estimation of the H2 gas utilization ratio using a BF shaft inner reaction simulator, Metall. Mater. Trans. B 51 (2) (2020) 417–421, http://dx.doi.org/10.1007/s11663-019-01768-w, URL http://link.springer.com/10.1007/s11663-019-01768-w.
- [14] C. Yilmaz, J. Wendelstorf, T. Turek, Modeling and simulation of hydrogen injection into a blast furnace to reduce carbon dioxide emissions, J. Clean. Prod. 154 (2017) 488–501, http://dx.doi.org/10.1016/j.jclepro.2017.03.162.
- [15] K. Ma, J. Deng, G. Wang, Q. Zhou, J. Xu, Utilization and impacts of hydrogen in the ironmaking processes: A review from lab-scale basics to industrial practices, Int. J. Hydrogen Energy 46 (52) (2021) 26646–26664, http://dx.doi.org/10. 1016/j.ijhydene.2021.05.095.
- [16] X. Jiang, L. Wang, F.M. Shen, Shaft furnace direct reduction technology Midrex and energiron, Adv. Mater. Res. 805–806 (2013) 654–659, http://dx. doi.org/10.4028/www.scientific.net/AMR.805-806.654.

- [17] K. Huitu, M. Helle, H. Helle, M. Kekkonen, H. Saxén, Optimization of midrex direct reduced iron use in ore-based steelmaking, Steel Res. Int. 86 (5) (2015) 456–465, http://dx.doi.org/10.1002/srin.201400091.
- [18] S. Lang, T. Haimi, M. Köpf, Circored fine ore direct reduction plus DRI smelting: Proven technologies for the transition towards green steel, in: F. Tesfaye, L. Zhang, D.P. Guillen, Z. Sun, A.A. Baba, N.R. Neelameggham, M. Zhang, D.E. Verhulst, S. Alam (Eds.), REWAS 2022: Energy Technologies and CO2 Management (Volume II), in: The Minerals, Metals & Materials Series, Springer International Publishing, Cham, 2022, pp. 61–71, http://dx.doi.org/10.1007/ 978-3-030-92559-8 7.
- [19] A. Carpenter, CO2 abatement in the iron and steel industry, IEA Clean Coal Centre 25 (2012) 193, URL https://usea.org/publication/co2-abatement-iron-and-steel-industry-ccc193.
- [20] M. Komatina, H.W. Gudenau, The sticking problem during direct reduction of fine iron ore in the fluidized bed, Met. J. Metall. 10 (4) (2004) 309– 328, http://dx.doi.org/10.30544/378, URL http://metall-mater-eng.com/index. php/home/article/view/378.
- [21] M. Choi, H. Sohn, Development of green suspension ironmaking technology based on hydrogen reduction of iron oxide concentrate: rate measurements, Ironmak. Steelmak. 37 (2) (2010) 81–88, http://dx.doi.org/10.1179/ 030192309X12506804200663.
- [22] A. Abdelghany, D.-Q. Fan, H. Sohn, Novel flash ironmaking technology based on iron ore concentrate and partial combustion of natural gas: a CFD study, Metall. Mater. Trans. B 51 (5) (2020) 2046–2056, http://dx.doi.org/10.1007/s11663-020-01909-6.
- [23] S. Li, H. Zhang, J. Nie, R. Dewil, J. Baeyens, Y. Deng, The direct reduction of iron ore with hydrogen, Sustainability 13 (16) (2021) 8866, http://dx.doi.org/ 10.3390/su13168866.
- [24] M.I. Boulos, The role of transport phenomena and modeling in the development of thermal plasma technology, Plasma Chem. Plasma Process. 36 (1) (2016) 3–28, http://dx.doi.org/10.1007/s11090-015-9660-7.
- [25] K.C. Sabat, A.B. Murphy, Hydrogen plasma processing of iron ore, Metall. Mater. Trans. B 48 (3) (2017) 1561–1594, http://dx.doi.org/10.1007/s11663-017-0957-1
- [26] M. Wolter, I. Levchenko, H. Kersten, K. Ostrikov, Hydrogen in plasmananofabrication: selective control of nanostructure heating and passivation, Appl. Phys. Lett. 96 (13) (2010) 133105, http://dx.doi.org/10.1063/1.3374324.
- [27] L. Mangolini, U. Kortshagen, Selective nanoparticle heating: another form of nonequilibrium in dusty plasmas, Phys. Rev. E 79 (2) (2009) 026405, http: //dx.doi.org/10.1103/PhysRevE.79.026405.
- [28] R. Gold, W. Sandall, P. Cheplick, D. MacRae, Plasma reduction of iron oxide with H and natural gas at 100 kW and 1 MW, Ironmak. Steelmak. 4 (1) (1977) 10–14.
- [29] A. Fridman, Plasma Chemistry, Cambridge University Press, 2008, http://dx.doi. org/10.1017/CBO9780511546075.
- [30] J.F. Plaul, W. Krieger, E. Bäck, Reduction of fine ores in argon-hydrogen plasma, Steel Res. Int. 76 (8) (2005) 548–554, http://dx.doi.org/10.1002/srin. 200506055.
- [31] T. Buergler, J. Prammer, Hydrogen steelmaking: Technology options and R&D projects, Berg- Huettenmaenn. Mon.hefte 164 (11) (2019) 447–451, http://dx.doi.org/10.1007/s00501-019-00908-8.
- [32] J.F. de la Fuente, A.A. Kiss, M.T. Radoiu, G.D. Stefanidis, Microwave plasma emerging technologies for chemical processes, J. Chem. Technol. Biotechnol. 92 (10) (2017) 2495–2505, http://dx.doi.org/10.1002/jctb.5205.
- [33] M. Kaiser, K.-M. Baumgärtner, A. Mattheus, Microwave plasma sources applications in industry, Contrib. Plasma Phys. 52 (7) (2012) 629–635, http: //dx.doi.org/10.1002/ctpp.201210059.
- [34] K. Sabat, R. Paramguru, B. Mishra, Reduction of oxide mixtures of (Fe₂O₃ + CuO) and (Fe₂O₃ + Co₃O₄) by low-temperature hydrogen plasma, Plasma Chem. Plasma Process. 37 (2017) 979–995, http://dx.doi.org/10.1007/s11090-017-9818-6.
- [35] P. Rajput, B. Bhoi, S. Sahoo, R.K. Paramguru, B.K. Mishra, Preliminary investigation into direct reduction of iron in low temperature hydrogen plasma, Ironmak. Steelmak. 40 (1) (2013) 61–68, http://dx.doi.org/10.1179/1743281212Y.0000000023, URL http://www.tandfonline.com/doi/full/10.1179/1743281212Y.0000000023.
- [36] P. Rajput, K.C. Sabat, R.K. Paramguru, B. Bhoi, B.K. Mishra, Direct reduction of iron in low temperature hydrogen plasma, Ironmak. Steelmak. 41 (10) (2014) 721–731, http://dx.doi.org/10.1179/1743281214Y.0000000186.
- [37] H.S. Uhm, Y.C. Hong, D.H. Shin, A microwave plasma torch and its applications, Plasma Sources. Sci. Technol. 15 (2) (2006) S26–S34, http://dx.doi.org/10.1088/ 0963-0252/15/2/s04.
- [38] B. Yeh, S. Chheda, S.D. Prinslow, A.S. Hoffman, J. Hong, J.E. Perez-Aguilar, S.R. Bare, C.C. Lu, L. Gagliardi, A. Bhan, Structure and site evolution of framework Ni species in MIL-127 MOFs for propylene oligomerization catalysis, J. Am. Chem. Soc. 145 (6) (2023) 3408–3418, http://dx.doi.org/10.1021/jacs.2c10551.
- [39] Omega-Engineering, Thermocouple response time, 2020, URL https://www.omega.com/en-us/resources/thermocouples-response-time.
- [40] C.R. Hubbard, R.L. Snyder, RIR measurement and use in quantitative XRD, Powder Diffr. 3 (2) (1988) 74–77, http://dx.doi.org/10.1017/ S0885715600013257.

- [41] D. Wagner, O. Devisme, F. Patisson, D. Ablitzer, A laboratory study of the reduction of iron oxides by hydrogen, 2008, http://dx.doi.org/10.48550/arXiv. 0803.2831, arXiv preprint arXiv:0803.2831.
- [42] H. Wang, H. Sohn, Effect of CaO and SiO2 on swelling and iron whisker formation during reduction of iron oxide compact, Ironmak. Steelmak. 38 (6) (2011) 447–452, http://dx.doi.org/10.1179/1743281211Y.00000000022.
- [43] A.G. Shashkov, A.F. Zolotukhina, L.P. Fokin, A.N. Kalashnikov, Transfer properties of mixtures of rarefied neutral gases. Hydrogen-argon system, J. Eng. Phys. Thermophys. 83 (1) (2010) 188–208, http://dx.doi.org/10.1007/s10891-010-0334-2.
- [44] E.L. Cussler, Diffusion: Mass Transfer in Fluid Systems, Cambridge University Press, 2009.
- [45] Y.F. Verolaĭnen, A.Y. Nikolaich, Radiative lifetimes of excited states of atoms, Sov. Phys. Uspekhi 25 (6) (1982) 431, http://dx.doi.org/10.1070/ PU1982v025n06ABEH004565.
- [46] C.D. Scott, S. Farhat, A. Gicquel, K. Hassouni, M. Lefebvre, Determining electron temperature and density in a hydrogen microwave plasma, J. Thermophys. Heat Transfer 10 (3) (1996) 426–435, http://dx.doi.org/10.2514/3.807.
- [47] A. Hjartarson, E. Thorsteinsson, J. Gudmundsson, Low pressure hydrogen discharges diluted with argon explored using a global model, Plasma Sources. Sci. Technol. 19 (6) (2010) 065008, http://dx.doi.org/10.1088/0963-0252/19/6/065008.
- [48] S. Wu, F. Wu, C. Liu, X. Liu, Y. Chen, T. Shao, C. Zhang, The effects of the tube diameter on the discharge ignition and the plasma properties of atmosphericpressure microplasma confined inside capillary, Plasma Process. Polym. 16 (3) (2019) 1800176, http://dx.doi.org/10.1002/ppap.201800176.
- [49] P. Middha, H. Wang, First-principle calculation for the high-temperature diffusion coefficients of small pairs: the H–Ar Case, Combust. Theory Model. 9 (2) (2005) 353–363, http://dx.doi.org/10.1080/13647830500098431.
- [50] C. Halstead, D.R. Jenkins, Rates of H+ H+ M→ H2+ M and H+ OH+ M→ H2O+ M reactions in flames, Combust. Flame 14 (3) (1970) 321–323, http://dx.doi.org/10.1016/S0010-2180(70)80046-3.
- [51] L. Walkauskas, F. Kaufman, Gas phase hydrogen atom recombination, Symp. (Int.) Combust. 15 (1) (1975) 691–699, http://dx.doi.org/10.1016/S0082-0784(75)80339-0, Fifteenth Symposium (International) on Combustion. URL https://www.sciencedirect.com/science/article/pii/S0082078475803390.
- [52] A. Hodges, A.L. Hoang, G. Tsekouras, K. Wagner, C.-Y. Lee, G.F. Swiegers, G.G. Wallace, A high-performance capillary-fed electrolysis cell promises more cost-competitive renewable hydrogen, Nat. Commun. 13 (1) (2022) 1304, http://dx.doi.org/10.1038/s41467-022-28953-x.
- [53] H.Y. Sohn, Energy consumption and CO2 emissions in ironmaking and development of a novel flash technology, Metals 10 (1) (2019) 54, http://dx.doi.org/ 10.3390/met10010054.
- [54] S. Li, Q. Kang, J. Baeyens, H. Zhang, Y. Deng, Hydrogen production: State of technology, in: IOP Conf. Ser. Earth Environ. Sci., 544, (1) IOP Publishing, 2020, 012011, http://dx.doi.org/10.1088/1755-1315/544/1/012011.
- [55] Y. Deng, S. Li, L. Appels, H. Zhang, N. Sweygers, J. Baeyens, R. Dewil, Steam reforming of ethanol by non-noble metal catalysts, Renew. Sustain. Energy Rev. 175 (2023) 113184, http://dx.doi.org/10.1016/j.rser.2023.113184.
- [56] F. Dawood, M. Anda, G. Shafiullah, Hydrogen production for energy: An overview, Int. J. Hydrogen Energy 45 (7) (2020) 3847–3869, http://dx.doi.org/ 10.1016/j.ijhydene.2019.12.059.
- [57] H. Song, S. Luo, H. Huang, B. Deng, J. Ye, Solar-driven hydrogen production: Recent advances, challenges, and future perspectives, ACS Energy Lett. 7 (3) (2022) 1043–1065, http://dx.doi.org/10.1021/acsenergylett.1c02591.
- [58] A.M. Oliveira, R.R. Beswick, Y. Yan, A green hydrogen economy for a renewable energy society, Curr. Opin. Chem. Eng. 33 (2021) 100701, http://dx.doi.org/10. 1016/j.coche.2021.100701.
- [59] D. Spreitzer, J. Schenk, Reduction of iron oxides with hydrogen—a review, Steel Res. Int. 90 (10) (2019) 1900108.
- [60] H. Hanumanthappa, H. Vardhan, G.R. Mandela, M. Kaza, R. Sah, B.K. Shanmugam, S. Pandiri, Investigation on iron ore grinding based on particle size distribution and liberation, Trans. Indian Inst. Met. 73 (2020) 1853–1866, http://dx.doi.org/10.1007/s12666-020-01999-5.
- [61] ITP-Mining, Energy and Environmental Profile of the US Mining Industry: Chapter 4: Iron, Tech. Rep., Department of Energy, Office of Energy Efficiency & Renewable Energy, 2002, URL https://www.energy.gov/sites/prod/files/2013/ 11/f4/iron.pdf.
- [62] J. Stubbles, Energy Use in the US Steel Industry: A Historical Perspective and Future Opportunities, Tech. Rep., Energetics, Inc., Columbia, MD (US), 2000, URL https://www.energy.gov/eere/amo/articles/itp-steel-energy-use-us-steel-industry-historical-perspective-and-future#:~:text=With%20an%20average% 20of%20770,2.
- [63] M. Elzohiery, H.Y. Sohn, Y. Mohassab, Kinetics of hydrogen reduction of magnetite concentrate particles in solid state relevant to flash ironmaking, Steel Res. Int. 88 (2) (2017) 1600133, http://dx.doi.org/10.1002/srin.201600133.
- [64] H. Baolin, H. Zhang, L. Hongzhong, Z. Qingshan, Study on kinetics of iron oxide reduction by hydrogen, Chin. J. Chem. Eng. 20 (1) (2012) 10–17, http: //dx.doi.org/10.1016/S1004-9541(12)60357-7.

- [65] D. Spreitzer, J. Schenk, Iron ore reduction by hydrogen using a laboratory scale fluidized bed reactor: Kinetic investigation—Experimental setup and method for determination, Metall. Mater. Trans. B 50 (5) (2019) 2471–2484, http: //dx.doi.org/10.1007/s11663-019-01650-9.
- [66] J. Feinman, Kinetics of hydrogen reduction of iron ore in a batch-fluidized bed. application to a three-bed continuous process, Ind. Eng. Chem. Process Des. Dev. 3 (3) (1964) 241–247, http://dx.doi.org/10.1021/i260011a011.
- [67] A. El-Geassy, M. Nasr, Influence of the original structure on the kinetics of hydrogen reduction of hematite compacts, Trans. Iron Steel Inst. Japan 28 (8) (1988) 650–658, http://dx.doi.org/10.2355/isijinternational1966.28.650.
- [68] S.K. Kuila, R. Chatterjee, D. Ghosh, Kinetics of hydrogen reduction of magnetite ore fines, Int. J. Hydrog. Energy 41 (22) (2016) 9256–9266, http://dx.doi.org/ 10.1016/j.ijhydene.2016.04.075.
- [69] O. Teplov, Kinetics of the low-temperature hydrogen reduction of magnetite concentrates, Russ. Metall. (Metally) 2012 (1) (2012) 8–21, http://dx.doi.org/ 10.1134/S0036029512010132.
- [70] M. Bahgat, M. Khedr, Reduction kinetics, magnetic behavior and morphological changes during reduction of magnetite single crystal, Mater. Sci. Eng. B 138 (3) (2007) 251–258, http://dx.doi.org/10.1016/j.mseb.2007.01.029.
- [71] A. Heikkilä, M. Iljana, H. Bartusch, T. Fabritius, Reduction of iron ore pellets, sinter, and lump ore under simulated blast furnace conditions, Steel Res. Int. 91 (11) (2020) 2000047, http://dx.doi.org/10.1002/srin.202000047.
- [72] K. Badr, Smelting of Iron Oxides Using Hydrogen Based Plasmas (Ph.D. thesis), University of Leoben, 2007.
- [73] T. Wolfinger, D. Spreitzer, J. Schenk, Analysis of the usability of iron ore ultrafines for hydrogen-based fluidized bed direct reduction—A review, Materials 15 (7) (2022) 2687, http://dx.doi.org/10.3390/ma15072687.